J|A|C|S
ARTICLES
Published on Web 04/03/2003

Lanthanum Strontium Manganite/Yttria-Stabilized Zirconia Nanocomposites Derived from a Surfactant Assisted, Co-assembled Mesoporous Phase

Marc Mamak,[†] Gabriella S. Métraux,[†] Srebri Petrov,[†] Neil Coombs,[†] Geoffrey A. Ozin,*[,†] and M. A. Green[‡]

Contribution from the Materials Chemistry Research Group, Chemistry Department, University of Toronto, 80 St. George St., Toronto, Ontario, Canada M5S 3H6, and Davy Faraday Research Laboratory, Royal Institution of Great Britain, 21 Albemarle Street, London, WIX 4BS United Kingdom, and Department of Chemistry, University College London, 20 Gordon Street, London, WC1H 0AJ United Kingdom

Received July 26, 2002; E-mail: gozin@chem.utoronto.ca

Abstract: A one-pot, soft-chemistry, surfactant-assisted co-assembly approach to prepare $La_{1-x}Sr_xMnO_3$ (LSM)/Y_2O_3-stabilized ZrO_2 (YSZ) nanocomposites for use as solid oxide fuel cell (SOFC) cathodes has been investigated. This material with sub-hundred nanometer grain sizes for each phase is the first such nanocomposite where aqueous-based precursors of each component are incorporated in a single synthetic step. This approach utilizes the co-assembly of an anionic yttrium/zirconium acetatoglycolate gel, cetyltrimethylammonium bromide as the cationic surfactant template, and inorganic La, Mn, and Sr salts under alkaline aqueous conditions. The resulting as-synthesized product is an amorphous mesostructured organic/inorganic composite, which is transformed to a mesoporous inorganic oxide with nanocrystalline YSZ walls upon calcination. Calcination to temperatures above 600 °C lead to collapse of the mesopores followed by further crystallization of the nanocrystalline YSZ phase and a final crystallization of the LSM perovskite phase above 1000 °C. Both the fully crystalline LSM/YSZ and the mesoporous intermediate phase have been investigated for phase homogeneity by TEM energy-dispersive X-ray spectroscopy (EDX) mapping and spot analysis which confirm the dispersion of LSM within a YSZ matrix at the nanometer scale. Impedance spectroscopy analysis of LSM/YSZ nanocomposite electrodes demonstrate a low polarization resistance of around 0.2 Ω cm^2 with an activation energy (E_a) as low as 1.42 eV. Cathodic polarization studies show stable current densities over a 40 h test demonstration.

Introduction

SOFCs are still a promising alternative power source to traditional mobile and stationary sources such as the internal combustion engine and coal burning power plants.[1] These fuel cells are based on an oxygen-ion conductor ceramic electrolyte such as yttria-stabilized zirconia (YSZ) and operate at the high temperature of 1000 °C. The main benefits of operating at such elevated temperatures are high efficiencies in converting chemical energy to electrical energy and the ability to directly process a multitude a fuels including hydrogen, methane, and butane. Currently, there is a drive toward developing intermediate operating temperature SOFCs (600 to 800 °C), however the lower temperature decreases the activity of the electrodes.[2] The classic electrode material and that most commonly employed on the cathode side (air electrode) of the fuel cell is the strontium-doped lanthanum manganite (LSM) perovskite. The electrochemical reaction of oxygen reduction at the cathode is generally agreed to occur at the interface between air, electronic conductor (LSM), and oxygen-ion conductor (YSZ) and is termed the triple-phase boundary (TPB).[3] Because pure LSM is a poor oxygen ion-conductor due to the lack of lattice oxygen vacancies and YSZ is an electronic insulator, most researchers have found composite electrodes of LSM and YSZ, which combine electronic and ionic conduction pathways, result in lower polarization losses at the cathode.[4] It is suggested that LSM/YSZ composite electrodes perform better due to the additional TPB sites created between LSM, YSZ, and air (pores) interfaces within the 3-D bulk of the electrode. Tailoring the

[†] Materials Chemistry Research Group, Chemistry Department, University of Toronto.
[‡] Davy Faraday Research Laboratory, Royal Institution of Great Britain and Department of Chemistry, University College London.

(1) (a) Minh, N. Q. *J. Am. Ceram. Soc.* **1993**, *76*, 563. (b) Ball, P. *Made to Measure, New Materials for the 21st Century*; Princeton University Press: Princeton, NJ, 1997. (c) Steele, B. C. H. *Nature* **1999**, *400*, 619.
(2) (a) de Souza, S.; Visco, S. J.; De Jonghe, L. C. *Solid State Ionics* **1998**, *98*, 57. (b) Irvine, J. T. S.; Sauvet, A. *Fuel Cells* **2001**, *1*, 205.
(3) Mogensen, M.; Primdahl, S.; Jørgensen, M. J.; Bagger, C. *J. Electroceramics* **2000**, *5*, 141.
(4) (a) Juhl, M.; Primdahl, S.; Manon, M.; Mogensen, M. *J. Power Sources* **1996**, *61*, 173. (b) Murray, E. P.; Tsai, T.; Barnett, S. A. *Solid State Ionics* **1998**, *110*, 235. (c) Kim, J.-D.; Kim, G.-D.; Moon, J.-W.; Lee, K.-L.; Kim, C.-E. *Solid State Ionics* **2000**, *133*, 67. (d) Jørgensen, M. J.; Primdahl, S.; Bagger, C.; Mogensen, M. *Solid State Ionics* **2001**, *139*, 1. (e) Kim, J.−D.; Kim, G.-D.; Moon, J.-W.; Park, Y.; Lee, W.-H.; Kobayashi, K.; Nagai, M.; Kim, C.-E. *Solid State Ionics* **2001**, *143*, 379. (f) Steele, B. C. H. *Solid State Ionics* **1997**, *94*, 239. (g) Østergard, M. J. L.; Clausen, C.; Bagger, C.; Mogensen, M. *Electrochim. Acta* **1995**, *40*, 1971. (h) Brant, M. C.; Matencio, T.; Dessemond, L.; Domingues, R. Z. *Chem. Mater.* **2001**, *13*, 3954.

microstructure of the composite electrode in terms of the relative particle size ratio as well as the volume ratio of components is important in controlling the TPB length as well as the continuity of the ionic/electronic conduction pathways.[3] Because the electrochemical reduction of O_2 is expected to occur within the first few microns from the electrolyte interface, researchers have used functional grading of the electrode in order to provide optimal cell performance. In this case, the first layer is often a 50:50 LSM:YSZ mixture composite and serves as the electrocatalytically active layer due to the large TPB length, whereas the outer layer(s) consist of pure LSM and provide for efficient current collection.[4g]

Virtually all LSM/YSZ composite electrodes to date can be described as a physical mixture of LSM and YSZ powders. Highly crystalline solid-state powders of each phase are first separately obtained through independent synthesis methods and then mixed by mechanical methods such as ball milling. Ball milling serves to decrease the particle size of each component, increasing the overall boundary region between each component, and thus increasing the overall TPB length while homogenizing the powder mixture. For electrolyte or anode supported cells, this intimately mixed powder is then combined with an organic vehicle such as glycerol or ethanol to form a slurry which can then be applied to a dense YSZ electrolyte substrate by techniques such as spraying, screen printing, spin coating, or simple hand painting. The typical particle size achieved for each component is on the order of one to several microns.

Although LSM/YSZ composites have been widely used as SOFC cathodes since 1980,[5] very few alternative methods for producing LSM/YSZ composites have been reported. To date, research interests in composite electrodes has mainly been limited to engineering methods in optimizing the TPB.[6] In one of two chemistry-based reports we have found, LSM/YSZ composite film electrodes were prepared by metal-organic decomposition from a single solution of all five elements.[7] Interestingly, this approach yields separate phase-pure products of LSM and YSZ without any unwanted byproducts. However, it appears that this method does not allow for facile tuning of the LSM to YSZ composition, as only a single LSM:YSZ ratio of 0.95:0.05 was reported. This ratio remains far from the optimal composition where percolation pathways of LSM and YSZ can coexist.[4c] Still, it was found that the addition of a small volume amount of YSZ was found to help suppress the growth of LSM particles upon sintering to high temperatures. The only other report of an alternative method for preparing LSM/YSZ composites, of which we are aware, utilizes a spray pyrolysis technique. In this method, a dispersion of 60 nm YSZ colloidal particles was added to an aqueous solution of La, Sr, and Mn salts and hydrogen peroxide.[8] The resulting mixture was then atomized to droplets, which are carried through a heating zone to form 1 μm spherical composite aggregates of TEM distinguishable phases of LSM and YSZ with grain sizes up to 100 nm.

On a different note, LSM composites have recently received attention due to interesting magnetic properties, some of which result when LSM is combined with an insulating inorganic oxide.[9] Mixed valent manganese oxides are known to exhibit colossal magnetoresistance (CMR) where the state of the material shows a transition from paramagnetic to ferromagnetic and is accompanied by a large change in electrical resistance.[10] The ferromagnetic mechanism can be described by the double-exchange process between Mn^{III} and Mn^{IV}. Interesting LSM composites include examples such as LSM/CeO_2 and LSM/$SrTiO_3$, which show improved properties such as enhanced room-temperature magnetoresistance effects.[11] These composites are physical mixtures and are prepared by methods similar to that described above. In an attempt to prepare a more homogeneous composite, one group has employed a solution phase chemical synthesis route to LSM/silica nanocomposites using a Si alkoxide and La^{3+}, Sr^{2+}, and Mn^{2+}/ethylenediaminetetraacetic acid (EDTA) complexes.[12]

The development of alternative chemical approaches toward composite electrode materials such as LSM/YSZ, where the molecular or sol precursors for each phase are incorporated in a single step, may prove to be successful in not only creating a macroscopically homogeneous composite material, but a nanostructured material, as the domain growth of either component may be effectively limited by the growth of the second component. Here, the fine nanoscale features of this composite would serve to increase the TPB density of the electrode. Additionally, nanostructured materials with dimensions of less than 100 nm have recently received much attention in solid-state ionics and related fields.[13] Enthusiasm about these materials arises from the fact that enhanced ionic and electronic conductivity plus other synergistic effects may become possible when the dimensions of grain size are reduced to the same order as the width of the grain boundary. As the grain size approaches the width of the grain boundaries, the accumulation of one vacancy type or electronic carrier in the space charge region could result in enhanced ionic or electronic conduction, respectively. This has been demonstrated by Maier in the case of nanoscale ion conductors where enhanced ionic conductivity was achieved due to the high density of grain boundaries, as grain boundary diffusion coefficients are often orders of magnitude greater than the bulk regions, and, more importantly, space charge effects.[14] Nanostructured materials amalgamated with porosity have great potential in the field of SOFCs and could lead to a better understanding of the electrode processes at hand.

The approach we describe in this paper for obtaining homogeneous LSM/YSZ nanocomposites is novel for the reason

(5) Takahashi, T.; Minh, N. Q. *Science and Technology of Ceramic Fuel Cells*; Elsevier: New York, 1995.
(6) (a) Tanner, C. W.; Fung, K.-Z.; Virkar, A. V. *J. Electrochem. Soc.* **1997**, *144*, 21. (b) Virkar, A. V.; Fung, K. Z. U. S. Patent 5, 543, 239, **1996**. (c) Ivers-Tiffée, E.; Weber, A.; Herbstritt, D. *J. Eur. Ceram. Soc.* **2001**, *21*, 1805.
(7) Hayashi, K.; Hosokawa, M.; Yoshida, T.; Ohya, Y.; Takahashi, Y.; Yamamoto, O.; Minoura, H. *Mater. Sci. Eng. B* **1997**, *B49*, 239.
(8) (a) Fukui, T.; Oobuchi, T.; Ikuhara, Y.; Ohara, S.; Kodera, K. *J. Am. Ceram. Soc.* **1997**, *80*, 261. (b) Fukui, T.; Ohara, S.; Naito, M.; Nogi, K. *J. Nanopart. Res.* **2001**, *3*, 171.
(9) Tokura, Y. *Curr. Opin. Solid State Mater. Sci.* **1998**, *3*, 175.
(10) (a) Ramirez, A. P. *J. Phys. Condens. Matter* **1997**, *9*, 8171. (b) Salamon, M. B.; Jaime, M. *Rev. Modern Phys.* **2001**, *73*, 583.
(11) (a) Balcells, Ll.; Carrillo, A. E.; Martinez, B.; Fontcuberta, J. *Appl. Phys. Lett.* **1999**, *74*, 4014. (b) Shlyakhtin, O. A.; Oh, Y. J.; Tretyakov, Y. D. *Solid State Commun.* **2001**, *17*, 261.
(12) Huang, Y.-H.; Yan, C.-H.; Wang, S.; Luo, F.; Wang, Z.-M.; Liao, C.−S.; Xu, G.-X. *J. Mater. Chem.* **2001**, *11*, 3296.
(13) (a) Verweij, H. *Adv. Mater.* **1998**, *10*, 1483. (b) Tuller, H. L. *J. Electroceram.* **1997**, *1*, 211. (c) Schoonman, J. *Solid State Ionics* **2000**, *135*, 5. (d) Knauth, P.; Tuller, H. L. *J. Am. Ceram. Soc.* **2002**, *85*, 1654.
(14) (a) Maier, J. *Prog. Solid State Chem.* **1995**, 171. (b) Sata, N.; Eberman, K.; Eberl, K.; Maier, J. *Nature* **2000**, *408*, 946.

that we start with no preformed LSM or YSZ particles, but employ a one pot chemical route using oligomeric and molecular precursors of each component, which are then assembled into a mesostructured organic/inorganic composite. A one-pot synthesis route to LSM/YSZ composites could, potentially, be technologically relevant as this would eliminate the need for 2 separate syntheses and high temperature calcination steps, hence lowering energy and time costs. The preparation of nanostructured SOFC electrodes remains an especially difficult task due to the high temperatures required in order to attach the electrode to the dense electrolyte (typically > 1100 °C for cathodes and 1400 °C for anodes in air) as well as the high operating temperature of the SOFC.[5] Under these high temperature oxidizing conditions, metal oxides readily sinter to form micron sized grains and larger agglomerates even when starting with nanoscale powders or sol−gel type precursors. Here, we demonstrate the use of a simple cationic surfactant to co-assemble anionic Y/Zr acetatoglycometalates with La, Sr, and Mn inorganic salts under alkaline aqueous conditions and low temperatures. This surfactant containing organic/inorganic composite yields a LSM/YSZ nanocomposite upon calcination to above 1000 °C. This general approach is loosely derived from our earlier reports of mesoporous nickel oxide-YSZ and mesoporous nickel-YSZ.[15] Mesoporous oxides have evolved as a distinct class of materials after receiving their genesis from MCM-41 and Mobil Oil Corporation in 1992 where silicates with periodic nanometer-dimensioned pores were formed using liquid crystal templating.[16] This approach has been rationally extended to transition metal oxides, which are more interesting in terms of electroactivity, catalysis, and magnetic properties as nicely summed up in a recent review by Antonelli.[17] Their large pore volume and high surface area are ideal for both catalysis and host−guest inclusion chemistry. We have previously demonstrated that mesoporous YSZ (*meso*-YSZ) as well as analogues containing Pt, NiO_{1+x}, and Ni, were thermally stable beyond 600 °C, which far supersedes all other mesoporous transition metal oxides, which we are aware of.[18] In this work, we believe that by incorporating both LSM and YSZ moieties in an initial as-synthesized mesostructured product we can achieve our goal of creating a homogeneous composite material with nanometer dimensioned grains potentially giving rise to a much larger TPB than conventionally prepared composite cathodes. Such a material can also be envisioned to display interesting ionic transport, electronic conductivity, and magnetic properties.

Experimental Section

(a) Preparation of *meso*-LSM-YSZ and nc-LSMYSZ. Yttrium−Zirconium acetatoglycolate gel (previously referred to as "YZr glycolate") was prepared exactly as previously reported in ref 18. The gel contained 16−18 atomic % Y. This viscous gel was added to a 100 mL high-density polypropylene bottle containing 30 mL water, 1 g cetyltrimethylammonium bromide (CTAB; Aldrich), and a variable amount of NaOH (typically 0.2 g to 0.6 g) while stirring the mixture rapidly with a magnetic stir bar. $MnCl_2 \cdot 4H_2O$, $La(NO_3)_3 \cdot 6H_2O$, and $Sr(NO_3)_2$ were predissolved in a minimum amount of water, then added quickly to the YZr acetatoglycolate/surfacant mixture while maintaining rapid stirring. Both the initial ratio of the Mn, La, and Sr salts and the basicity of the initial YZr acetatoglycolate/surfactant mixture were found to control the final LSM phase, stoichiometry, and impurity phases. We have determined that the approximate molar ratio of 1 Mn: 0.34−0.42 La: 0.24−0.30 Sr leads to a final phase having a stoichiometry close to $La_{0.7}Sr_{0.3}MnO_3$ due to incomplete precipitation of manganese hydroxide which is evident by the slightly pink supernatant. An initial pH of 12.5 appears to be optimal for both mesophase formation and precipitation in the desired ratio of Mn, La, and Sr reagents. Each polypropylene bottle is stirred for at least 30 min after all reagents have been added to ensure homogeneity and unwanted precipitates. The bottles were incubated overnight at 60 °C (incubation times longer than this did not seem to have any effect upon the product), cooled, and filtered by vacuum filtration yielding the material, which we refer to as "as-synthesized *meso*-LSM-YSZ". The resulting material was initially dark purple to black in color and waxy in consistency, turning slightly more brown, more plastic-like and brittle after drying. Calcination to 450 °C in air (6 h ramp from RT, held at 450 °C for 1 h) yielded a brown, single-phase material, denoted "*meso*-LSM-YSZ". This brown powder became black after heating to temperatures around 1000 °C. All materials sintered to above 1000 °C will be referred to as "nc-LSMYSZ".

(b) Control Reaction A. The exact procedure was followed in experimental part (a) except YZr acetatoglycolate gel was excluded from the reaction mixture. A black powder, which we will refer to as LSMO, was obtained after calcination to 1100 °C and was used for subsequent powder X-ray phase analysis as further described in the text.

(c) Control Reaction B. The exact procedure was followed in experimental part (a) except CTAB was excluded from the reaction mixture.

(d) Preparation of $La_{0.7}Sr_{0.3}MnO_3$ by the Pechini Method. For a direct powder X-ray diffraction phase comparison with nc-LSMYSZ, a powder sample of $La_{0.7}Sr_{0.3}MnO_3$ (also referred to as LSMO) was prepared from an adaptation of the synthesis described in ref 19.[19] The inorganic salts of $MnCl_2 \cdot 4H_2O$, $La(NO_3)_3 \cdot 6H_2O$, and $SrCl_2 \cdot 6H_2O$ were added in a 1:0.7:0.3 ratio (0.38 g, 0.60 g, and 0.16 g, respectively) to a beaker containing a solution of 28.8 g citric acid predissolved in 36 mL water, which was stirred at 60 °C. After stirring at 60 °C for about 2 h, 24.8 g of ethylene glycol was added, then the temperature was increased to 90 °C for about 5 h. The resulting resin was calcined to 1100 °C in air to yield a fine black powder.

(e) Powder X-ray (PXRD) Characterization of nc-LSMYSZ and Pure Perovskite $La_{1-x}Sr_xMnO_3$. PXRD measurements were carried out on a Siemens D 5000 Diffractometer System, using a linear focused Cu Kα target, operating at 50 kV/35mA. The secondary beam was monochromatized by a Kevex Solid State detector. Step scan mode was used for all scans and the data was further processed by DiffracPlus software. Phase identification was made using PDF-2 Database, set 1−47, 1998. For perovskite material indexing and lattice parameters, refining procedures were initially performed by Winindex and Winmetric routines as parts of DiffracPlus. An additional refinement with Full Profile Fitting method was applied using PowderCell−beta version[20] for checking the indexing and for quantification of the identified phases in different analyzed materials. The peak profile deconvolution for particle size determination was done with Topas P Bruker AXS software package using the Fundamental Paramenter Approach (FPA).[21] The starting structural models used as input data for the identified phases in both PowderCell−beta and GSAS[22] code

(15) Mamak, M.; Coombs, N.; Ozin, G. A. *Chem. Mater.* **2001**, *13*, 3564.
(16) (a)Kresge, C. T.; Leonowicz, M. E.; Roth, W. J.; Vartuli, J. C.; Beck, J. S. *Nature* **1992**, *359*, 710. (b) Beck, J. S.; Vartuli, J. C.; Roth, W. J.; Leonowicz, M. E.; Kresge, C. T.; Schmitt, K. D.; Chu, C. T.-W.; Olson, D. H.; Sheppard, E. W.; McCullen, S. B.; Higgins, J. B.; Schlenker, J. L. *J. Am. Chem. Soc.* **1992**, *114*, 10 834.
(17) He, X.; Antonelli, D. *Angew. Chem., Int. Ed.* **2002**, *41*, 214.
(18) (a) Mamak, M.; Coombs, N.; Ozin, G. *Adv. Mater.* **2000**, *12*, 198. (b) Mamak, M.; Coombs, N.; Ozin, G. *J. Am. Chem. Soc.* **2000**, *122*, 8932. (c) Mamak, M.; Coombs, N.; Ozin, G. A. *Adv. Funct. Mater.* **2001**, *11*, 59.
(19) Kakihana, M.; Arima, M.; Yoshimura, M.; Ikeda, N.; Sugitani, Y. *J. Alloys and Compounds* **1999**, *283*, 102.
(20) PowderCell 3.2, beta. W. Kraus and G. Nolze, 2000, BAM, Berlin.

were taken from ICSD Database.[23] Six reflections from the cubic YSZ-oxide and 13 from the Perovskite LSMO were used. We assumed that the phase system was cooled slowly enough to be in equilibrium and no lattice microstrain could be imposed on both crystalline phases: YSZ and LSMO.

(f) Physical Characterization of *meso*-LSM-YSZ and nc-LSMYSZ. Low-angle powder X-ray diffraction (PXRD) was performed on a Siemens D5000 diffractometer using Cu Kα radiation ($\lambda = 1.54178$ Å) with a Kevex 2005−22 solid-state detector. Transmission Electron Microscopy (TEM) imaging and energy-dispersive X-ray spectroscopy (EDX) were performed using Technai 20 TEM at the accelerating voltage of 200 kV. Samples were embedded in an epoxy-based resin, cured at 60 °C for 24 h and sectioned using an ultra-microtome and a diamond knife to a thickness of approximately 60 nm. The thin sections were then mounted on a copper grid. Alternatively, high resolution-field emission-scanning transmission electron microscopy (HR−FE-STEM) imaging and EDX were done on a JEOL 210F field emission microscope operating at an accelerating voltage of 200 kV. Thermal Gravimetric Analysis (TGA) was done at 5°/min in air on a Netzsch STA-409 DTA with simultaneous TGA. Nitrogen adsorption/desorption isotherms were performed at 77 K. All samples were outgassed at 200 °C. Average pore diameters were determined using the BJH method using the desorption isotherm branch. Elemental analyses of powder samples were performed by X-ray Florescence (XRF) on a Philips 2404, 4kW sequential XRF. Samples were suspended on 6 micron Mylar film and the Philips Semiquantitative software was used. Magnetic susceptibility measurements were performed using a Quantum Design MPMS7 SQUID magnetometer.

(g) Electrochemical Study. All powder samples were sintered onto dense 250 μm thick YSZ electrolyte substrates. All nc-LSMYSZ samples were finely ground with a mortar and pestle, then made into ink by adding glycerol. Symmetrical cells were made by hand painting the ink onto both sides of the YSZ substrate. For physical mixture samples, commercial powders of $La_{0.7}Sr_{0.3}MnO_3$ (99.9%, 1−10 μm particle size, Marketech International, Inc.) and 8 mol % Y_2O_3-stabilized ZrO_2 (Tosoh Corp.) were finely ground in a mortar and pestle, then slurried with glycerol and painted onto both sides of the YSZ substrate. The area and thickness of all electrodes were kept constant within human error. Both nc-LSMYSZ samples and physical mixtures of LSM/YSZ were fired onto the YSZ substrate at 1100 °C for 2 h in air. Electrical contact to the fired samples was achieved by affixing Pt mesh with Pt ink (Engelhard, #6082). The lead Pt wires were kept the same for all samples. Impedance spectroscopy measurements were made on the symmetrical cells in a tube furnace in air using a Solartron 1260 frequency response analyzer and a Solartron 1287 potentiostat/galvanostat. All samples were analyzed in symmetrical cells from 0.1 to 10^7 Hz at temperatures from 400 °C to 800 °C using an ac amplitude of 30 mV. Automated acquisition was facilitated by ZPLOT/ZVIEW and CorrWare (Scribner Associates) software.

The stability of our nc-LSMYSZ electrode was examined under cathodic polarization using a three-electrode cell configuration denoted as nc-LSMYSZ/YSZ/Pt and illustrated in Scheme 1. The geometrical area of the nc-LSMYSZ electrode was approximately 0.6 cm in diameter (0.28 cm^2). On the opposite side of the dense YSZ, platinum counter and reference electrodes of 1000 Å thickness were deposited by RF sputtering with the respective approximate areas of 0.45 cm^2 and 0.06 cm^2. Electrical contact to the nc-LSMYSZ electrode was achieved by affixing Pt mesh and gold ink (Engelhard, #A3360), whereas platinum ink (Engelhard, #6082) was used to affix Pt mesh to the sputtered counter and reference electrodes. Gold ink was used at the working electrode since it is well-known to have lesser oxygen activating properties than platinum, and would thus, have less influence on our results. In a box furnace at 800 °C in air, a voltage of −0.3V was applied versus the reference electrode in order to reduce gaseous oxygen (O_2) to oxide anions (O^{2-}) at the air/nc-LSMYSZ/YSZ interface. Over a period of 2 d, we measured the current density of the cell as a function of operation time at −0.3 V. At selected points during the operation, impedance spectra were collected at the applied voltage of −0.3 V (ac amplitude: 10 mV) and at open circuit conditions (ac amplitude: 20 mV).

Scheme 1. Experimental Cell Design for Cathodic Polarization Measurements

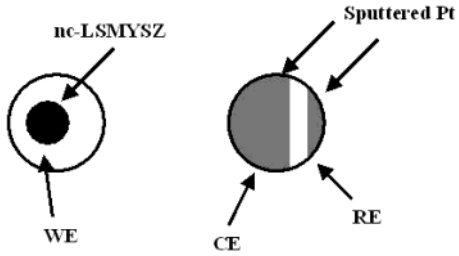

Results and Discussion

As-synthesized *meso*-LSM-YSZ materials were prepared using a surfactant assisted co-assembly method where the cationic surfactant, cetyltrimethylammonium bromide (CTAB), assembles the negatively charged yttrium−zirconium acetatoglycolate gel with La^{3+}, Sr^{2+}, and Mn^{2+} moieties into a mesophase under alkaline aqueous conditions. Figure 1(a) shows the low-angle PXRD pattern of the as-synthesized material giving a first *d* spacing of about 42 Å, which is typical for CTAB assembled materials including MCM-41 as well as our pure *meso*-YSZ. Upon calcination to 450 °C, the surfactant and remnant acetate/glycol ligands are removed, and the low-angle reflection is slightly diminished in intensity and shifted to lower *d* spacing. TGA shows a weight loss of about 50 wt % due to loss of surfactant, acetate and glycol ligands, and hydroxyl groups. This first reflection is relatively broader than that observed for pure *meso*-YSZ materials, indicating that the addition of LSM precursors results in a less ordered mesopore network. Incremental heating to higher temperatures leads to an expansion in the first *d* spacing before a final loss of low-angle reflection intensity near 650 °C. The initial decrease in *d* spacing reflects a contraction in the average pore-wall to pore-wall distance resulting from condensation of the pore walls when going from a partially hydrolyzed, amorphous organic/inorganic composite to a fully inorganic nanocrystalline YSZ-based framework. At temperatures higher than 450 °C, we believe the pore walls further crystallize, as YSZ grains grow larger through sintering at the grain boundaries, making denser walls and resulting in larger pores. Eventually, this grain growth leads to collapse of the mesopores. Some variation of the first *d* spacing is observed with the degree of LSM loading, leading to a larger *d* spacing at higher loadings. The PXRD patterns in Figure 1(b) show the high-angle region of *meso*-LSM-YSZ calcined at incremental temperatures where broad reflections are observed due to the nanocrystalline cubic YSZ phase. At lower calcination temperatures, only a broad peak at around 30° 2θ is observed due to overlap of 111 and 200 reflections. The peakwidth is consistent with a YSZ crystallite size less than 30 Å as we have investigated by thorough HR−FE-TEM analysis. No LSM perovskite or impurity phases are evident below 800 °C.

A representative Type IV nitrogen adsorption isotherm giving a BET surface area of 107 m^2/g for *meso*-LSM-YSZ calcined

(21) Topas P V 1.0. Profile Fitting using an Analytical as well as an Fundamental Parameters Approach. 1998. Bruker AXS, Karlsruhe, Germany.
(22) General Structure Analysis System. A. C. Larson & B. Von Dreele, Los Alamos NL, 1985−1997.
(23) Inorganic Crystal Structures Data, 2000−2, FIZ Karlsruhe, Germany.

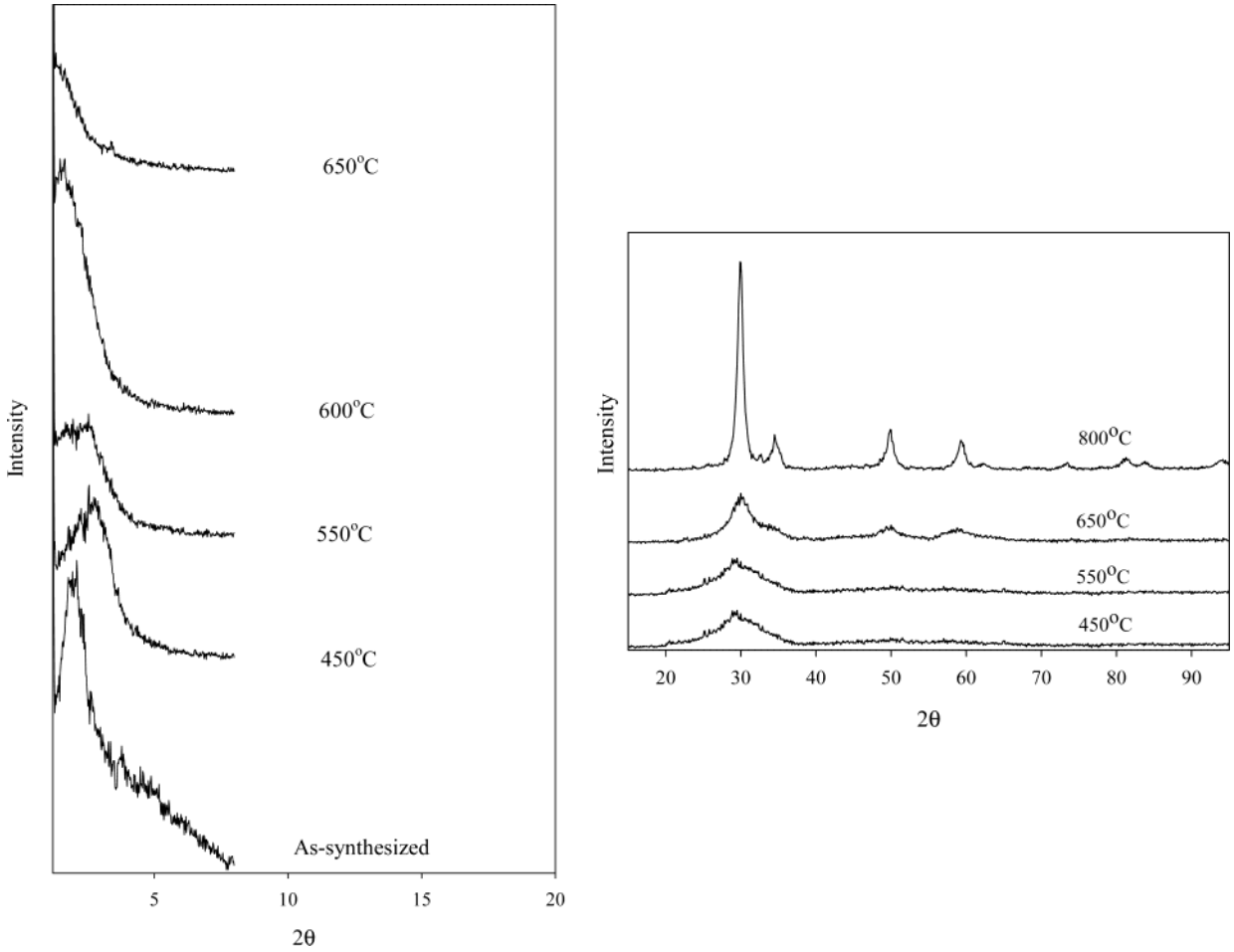

Figure 1. (a) Left: Low-angle PXRD patterns for *meso*-LSM-YSZ in as-synthesized and calcined forms. (b) Right: High-angle PXRD patterns for calcined *meso*-LSM-YSZ at different temperatures.

at 450 °C is shown in Figure 2, top which is to be contrasted with the pseudo-Type I isotherm for *meso*-YSZ (BET surface area = 260 m^2/g). *Meso*-YSZ has been previously determined to have pores near the micro-/meso-regimes, 18−20 Å, which results in dramatic gas uptake at low partial pressures.[24] The addition of La^{3+}, Sr^{2+}, and Mn^{2+} moieties perturbs mesophase formation by giving rise to much larger pores and a decreased BET surface area, both effects we have previously examined more in depth for *meso*-NiO_{1+x}-YSZ systems. Incremental higher loadings of either LSM or NiO_{1+x} further widen pores leading to significant nitrogen uptake at higher partial pressures with a hysteresis loop formed from the adsorption and desorption isotherm branches, both characteristic of Type IV mesoporous materials. As shown in the Figure 2, top inset, an average pore diameter of 40 Å is observed for a sample containing about 40 wt % LSM as calculated from the desorption branch.

The TEM micrograph of *meso*-LSM-YSZ calcined at 450 °C shown in Figure 2, bottom shows a mesoporous material with an average pore diameter consistent with gas adsorption analysis. This material has the classic worm-hole structure with a random network of pores as now described by many researchers.[25] The high viscosity of our yttrium−zirconium acetatoglycolate gel with the precipitation of La^{3+}, Sr^{2+}, and Mn^{2+} salts and high stirring rate with a magnetic stir bar most probably effects the CTAB directed co-organization of the mesophase and leads to this disordered network of pores rather than an organized liquid crystalline phase. EDX spot analysis and elemental mapping show this material to be quite homogeneous in terms of elemental distribution, an issue we shall return to when discussing sintered *meso*-LSM-YSZ, denoted nc-LSMYSZ.

The experimental powder X-ray diffraction data for nc-LSMYSZ, purposely composed of the two phases $(Y_xZr_{1-x})O_2$ and $La_{1-x}Sr_xMnO_3$, was directly compared to that of pure perovskite powders of similar stoichiometry, $La_{1-x}Sr_xMnO_3$ where $x \approx 0.2-0.3$ (referred in the text as LSMO), which were independently synthesized by methods described in the Experimental Sections (b) and (d). The synthesized perovskite material, denoted as LSMO, appears with a high degree of crystallinity and is associated with occurrence of a minor (7.2 wt %) phase with the composition of a defect spinel—Mn_3O_4, I 4_1/amd, shown in Figure 3, top. Typical $La_{1-x}Sr_xMnO_3$ perovskite materials (LSMO's) are known to appear with different symmetry according to their stoichiometry (values of x), A:B cation ratio, (A + B):O ratio, and the Goldschmidt tolerance factor t for ABO_3 perovskites. Trigonal, R $\bar{3}$C, monoclinic, P 2/c, orthorhombic, P bnm and P 222_1, and tetragonal, I 4/mcm, structures are all reported in the literature.[26] The diffraction data from our LSMO perovskite was successfully indexed in both rhombohedral (TREOR algorithm) and monoclinic (ITO algorithm)

(24) Kruk, M.; Jaroniec, M. *Chem. Mater.* **2001**, *13*, 3169.
(25) (a) Tanev, P. T.; Pinnavaia, T. J. *Science* **1995**, *267*, 865. (b) Zhang, W.; Pauly, T. R.; Pinnavaia, T. J. *Chem. Mater.* **1997**, *9*, 2491.
(26) Zheng, F.; Pederson, L. R. *J. Electrochem. Soc.* **1999**, *146*, 2810.

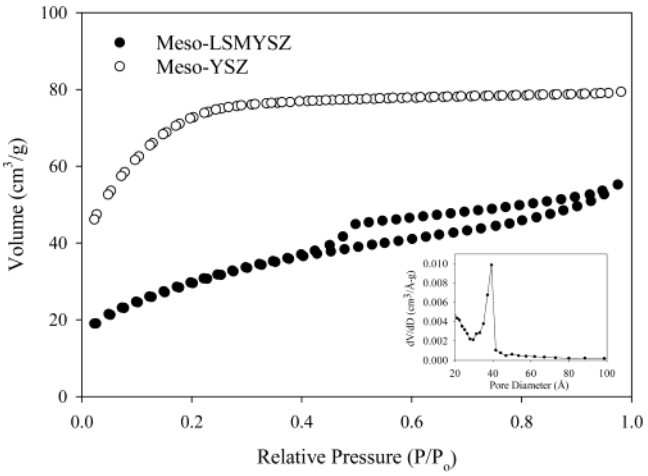

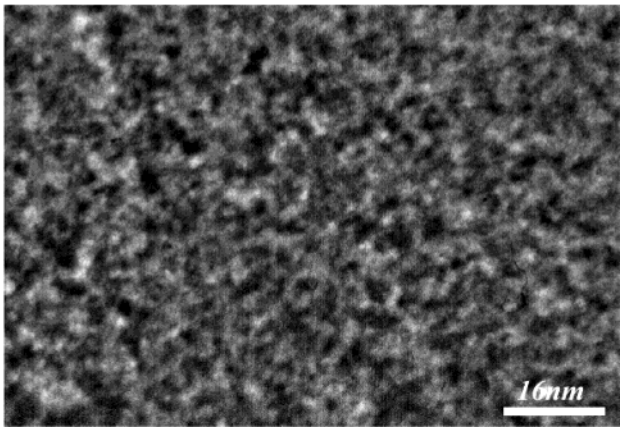

Figure 2. Top: Nitrogen adsorption/desorption isotherms comparing *meso*-YSZ and *meso*-LSM-YSZ both calcined at 450 °C. Top Inset: pore size distribution using the BJH method of the desorption isotherm branch for *meso*-LSM-YSZ. Bottom: TEM micrograph of a *meso*-LSM-YSZ thin section.

Table 1. Diffraction Data for LSMO Perovskite Phase

R $\bar{3}$C	*I* 2/*a*
$a = 5.51567(21)$ Å	$a = 7.77961(73)$ Å
	$b = 5.51456(41)$ Å
$c = 13.3689(6)$ Å	$c = 5.47784(60)$ Å
	$\beta = 90.62(1)°$
$V = 352.2(2)$ Å^3	$V = 235.41(9)$ Å^3
$Z = 6$	$Z = 4$
$M_{20} = 28$ (31, 0.0042)	$M_{20} = 28$ (92, 0.0602)

lattices as shown in Table 1. Lattices of these two types are commonly reported for La, Sr, Mn perovskites. In fact, the smaller monoclinic cell can be easily evaluated from the larger trigonal/hexagonal lattice as both represent the same arrangement of structural units, Figure 3, bottom. However, based on our analysis, we have concluded that our LSMO perovskite is hexagonal as it also matches very well with the recent X-ray powder data for $La_{0.65}Sr_{0.35}MnO_3$.[27] The GOF for monoclinic I 2/a compared to hexagonal R $\bar{3}$C is mainly due to the better statistics based on the greater number of calculated reflections for the monoclinic cell.

Our first synthetic attempts at nc-LSM-YSZ composites resulted in a large excess of lanthanum, as evident from XRF analysis, in the stoichiometry of our final material due to the incomplete precipitation of manganese hydroxide during the initial synthesis. PXRD analysis of these first materials, Figure 4, top, showed the presence of three major phases: the desired phase of cubic YSZ, a cubic oxide phase which is most likely (La,Mn)O with the NaCl type of structure, and a nonidentified La−Mn−O phase which appears similar to the side products described by Zheng and Pederson.[26,28] The desired LSM perovskite phase was not observed to be present in materials made from these initial syntheses. Upon improving the stoichiometry of our material through decreasing the relative amount of La^{3+}, the sintered *meso*-material, nc-LSMYSZ, was now found to be composed of two major phases: cubic $(Y_xZr_{1-x})O_2$ and hexagonal (R $\bar{3}$C) perovskite-type $La_{1-x}Sr_xMnO_3$, as seen in Figure 4, bottom. There are a minor amount of impurities, most likely complex La,Mn-oxides, frequently observed as associated phases[26] as well as a cubic $(Mn,La)_2O_3$ Bixbyite phase. The full-pattern-fitting-method (PowderCell-beta) was used for quantification of the abundance of the two major phases, thus eliminating the need for the appropriate standards and to allow all peaks to be included in the quantitative procedure. The results show nc-LSMYSZ to be composed of 51 wt % LSM hexagonal perovskite phase, about 44 wt % YSZ cubic oxide phase, and about 5 wt % cubic $(Mn,La)_2O_3$. The real amounts should be slightly lower due to the presence of the other impurity phase(s), but should not change the relative ratio between the two major phases.

One of the important characteristics of the mesoporous-derived material, nc-LSMYSZ, was the average particle size. The average particle sizes for the $La_{1-x}Sr_xMnO_3$ phase were determined by the FPA approach and are presented in Table 2. For the purpose of direct comparison, a particle size determination is also presented for a sample of pure mesoporous-YSZ, which was subjected to identical heat treatment (3 h at 1050 °C) as the nc-LSMYSZ sample. In the nc-LSMYSZ sample, both the YSZ and LSM phases are of very similar average particle size, resulting in sub-hundred nanometer crystallite size. The average particle size for the YSZ phase reflections of meso-YSZ are many times greater than that of the YSZ phase in the composite material, nc-LSMYSZ. This evidence suggests that the YSZ grain growth and crystallization is inhibited by the incorporation of the LSM phase into the YSZ mesophase resulting in a composite material of nanodimensions.

In Figure 5 we show HR−FE-TEM micrographs and EDX spot analysis spectra which are representative of nc-LSMYSZ. Our EDX spot analysis compares two regions of the sample we observed to be of slight difference in phase contrast, denoted as phase P and phase YSZ. The corresponding spectrum for phase P shows that La, Mn, Sr, Y, and Zr elements are all

(27) Paiva-Santos, C. O.; Marques, R. F. C.; Jafelicci, M.; Varanda, L. C. *Powder Diffraction* **2002**, *17*, 149.

(28) Note: Regarding the NaCl-type of (La, Mn)O phase, it is worth to mention that both La and Mn elements are reported to form such type of oxide phases. MnO is well known as having such an Fcc (VI−VI) type structure ($a = 4.445$ Å) based on the appropriate ionic radii ratio of $R = 0.51$, which emphasizes an octahedral packing for both ions. As for LaO, a cubic close packing arrangement is unusual due to the larger size of La ($R = 0.79$). Nevertheless, such a structure for LaO is reported (Leger, J. M.; Yacoubi, N.; Loriers, J. *J. Solid State Chemistry* **1981**, *36*, 261) and an Fcc diffraction pattern with $a = 5.14$ Å is assigned as PDF-2 # 33−0716. All 4 peaks marked with "O" were indexed very well with the cubic *Fm*3*m* lattice with a cell parameter of 4.754(3) Å. Assuming a linear dependence of cell parameter as a function of the La-content in the unit cell, one may estimate an approximate La content of 0.4 and an overall chemical composition of $Mn_{0.6}La_{0.4}O$. Regarding the "x" phase, it could be an intermediate tetragonal/orthorhombic phase with the composition of $La_3Mn_2O_7$ or $LaMn_2O_4$ or La_2MnO_4 similar to those described in the above-mentioned work of Zheng and Pederson.

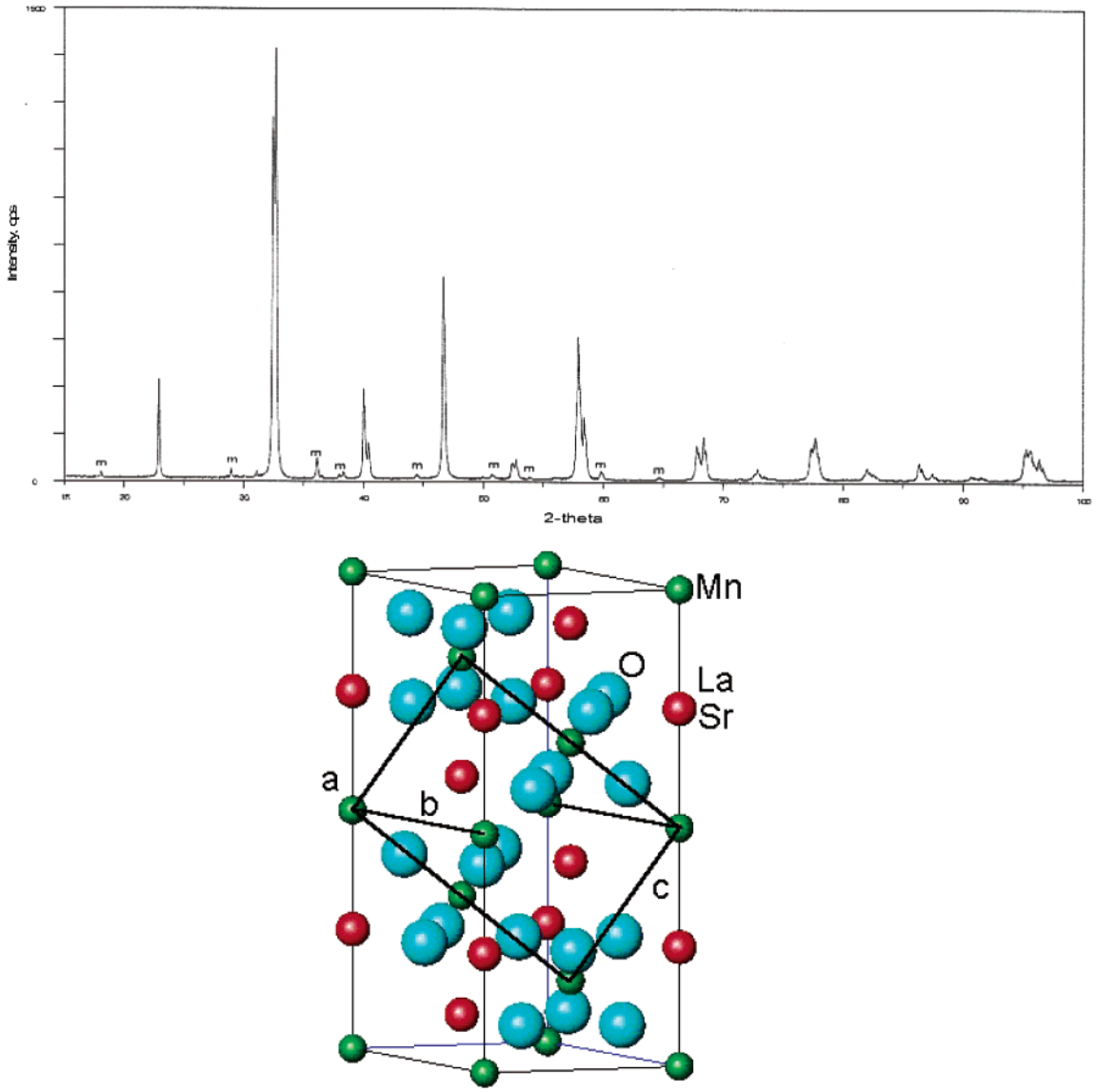

Figure 3. Top: Powder X-ray diffraction data for pure perovskite, LSMO. This data was used for its structural chracterization. "m" represents the minor phase of Mn_3O_4. Bottom: Illustration of the relationship between the two lattices where the monoclinic I 2/a cell is enclosed in the larger hexagonal R $\bar{3}$ C lattice. They both shared a common *b*-axis (5.516 Å). The monoclinic cell is almost orthogonal (beta = 89.38°).

present for the spot selected where the relative ratios of La:Sr: Mn and Y:Zr are in close agreement with the bulk elemental analysis technique of XRF. The corresponding EDX spectrum of phase YSZ shows major peaks from Zr, Y, and Mn, whereas La and Sr peaks are almost indistinguishable from the background signal. After thorough analysis of the thin-sectioned sample, it is evident that Y and Zr are present throughout the sample, whereas, La, Sr, and Mn are concentrated in 50−100 nm domains, and these are dispersed throughout the sample. These domain sizes correspond remarkably well with our crystallite size determination from our PXRD analysis presented above in Table 2. Because Mn is present, albeit in low amounts compared to Y and Zr, in the regions deficient in La and Sr, it may behave either as a solid solution with YSZ or as the separate phase Mn_2O_3, as observed in the PXRD plot represented in Figure 4, bottom. Reports indicate that Mn is soluble in YSZ up to 5 mol % at 1000 °C or about 7 mol % at 1100 °C, and results in a small decrease in the lattice parameters for YSZ.[29,30] We, however, do not see any discernible lattice contraction for our composite YSZ phase versus pure mesoporous-YSZ. These results may indicate the coexistence of a very slightly Mn-doped YSZ phase along with a minor phase of Mn_2O_3. EDX mapping (Figure 6) gives additional evidence showing a uniformly high concentration of Zr throughout the sample, whereas Mn and La (Sr was not analyzed) coexist in sub-hundred nanometer domains. The Mn and La rich domains appear well dispersed throughout the thin section and appear to have random connectivity in the YSZ matrix.

Although it is difficult to directly probe the mechanism of formation for as-synthesized *meso*-LSM-YSZ, it is evident that the charge association of oppositely charged CTAB and yttrium−zirconium acetatoglycolate is the main structure directing tandem responsible for the formation of the mesophase and subsequent cocrystallization of phase pure YSZ and LSM phases. Suib et al. previously synthesized mesoporous manga-

(29) (a) Yokokawa, H.; Sakai, N.; Kawada, T.; Dokiya, M. In *Proceedings of the 2nd International Symposium on Solid Oxide Fuel Cells*; Grosz, F., Zegers, P., Singhal, S. C., Yamamoto, O., Eds.; CEC: Luxembourg, 1991; p 663. (b) Appel, C. C.; Bonanos, N.; Horsewell, A.; Linderoth, S. *J Mater. Sci.* **2001**, *36*, 4493.
(30) Mitterdorfer, A.; Gauckler, L. J. *Solid State Ionics* **1998**, *111*, 185.

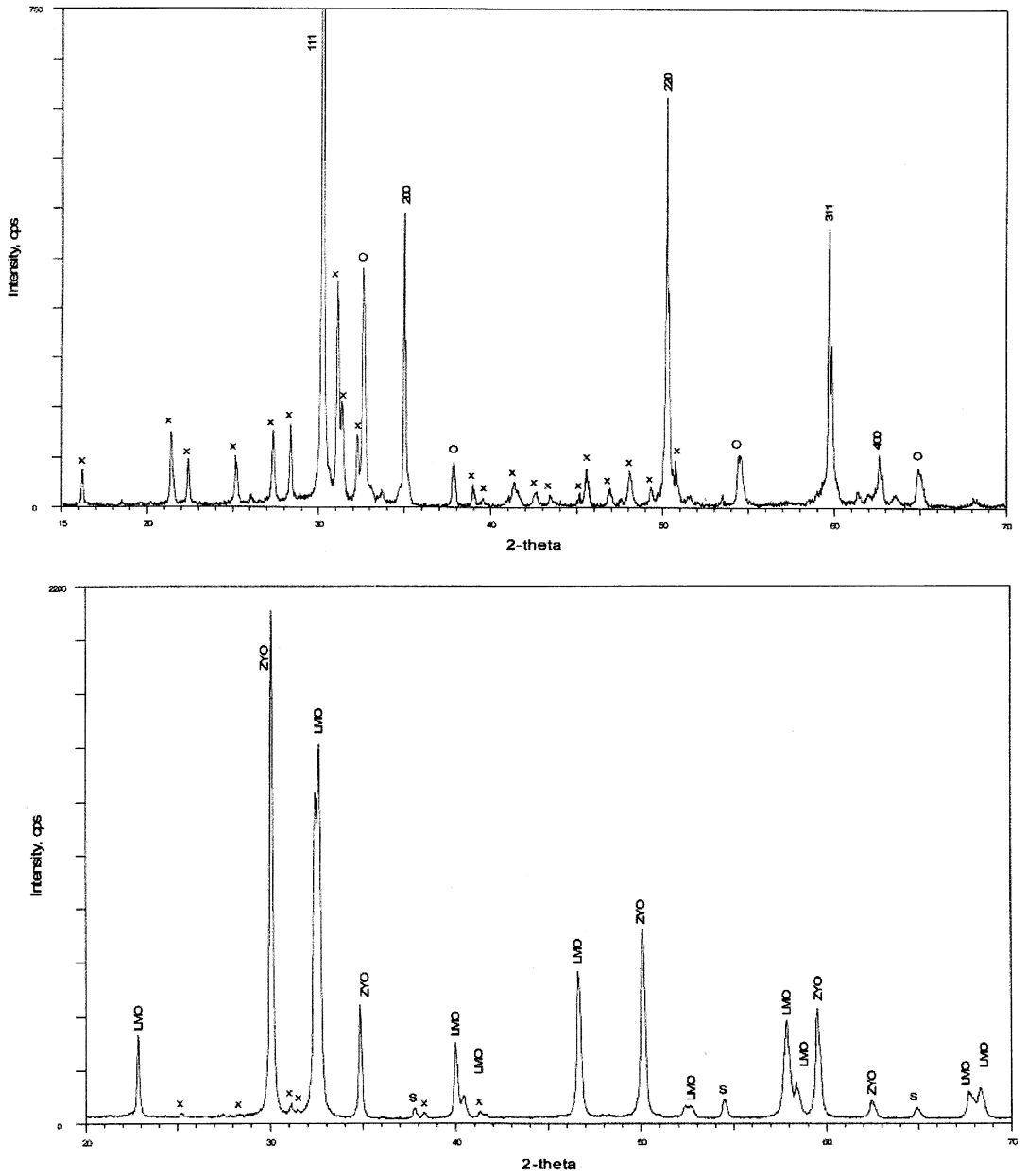

Figure 4. PXRD patterns comparing nc-LSMYSZ containing a large excess of lanthanum (Top) with an optimized synthesis (Bottom). Top: cubic YSZ phase peaks are marked with their indices in a *Fm*3*m* lattice, "O" represents a cubic oxide phase most likely (La,Mn)O with a NaCl type of structure, "x" represents a nonidentified La−Mn−O phase close to the side products described in ref 26. Bottom: ZYO − the cubic YSZ phase, LMO—the perovskite phase, $LaMnO_3$, S—the peaks from the cubic $(Mn,La)_2O_3$ Bixbyite C solid solution phase, x—the complex La,Mn-oxide impurity phase(s).

nese oxides using the reagents of CTAB, $MnCl_2$, and NaOH, however, our "control experiment A" demonstrates that only dense, nonmesoporous phases of La, Sr, and Mn are precipitated as poorly crystalline or amorphous hydroxides when the YZr acetatoglycolate is excluded from the reaction mixture.[31] Our synthesis conditions include a different order of addition of precursors, higher water to $MnCl_2$ ratio, and lower CTAB concentrations, all of which differ significantly from Suib's preparation, hence our result was not unexpected. The PXRD of the as-synthesized product from "control reaction A" shows a distinct peak at 19.5° 2θ, which can be attributed to β-MnOOH, also known as feitknechtite (JCPDS card 18-0804).[32] Upon calcination to above 1000 °C, the rhombohedral phase of LSM perovskite is observed as the major phase along with a minor Mn_3O_4 impurity phase. This LSM phase is identical to the LSM phase observed nc-LSMYSZ samples. At exceedingly high initial loadings (greater than 80 wt %) of La/Sr/Mn salts in the *meso*-LSM-YSZ preparation, a visible phase separation occurs leading to the precipitation of a variety of undesirable dense phases without any formation of the desired mesophase. After initiation, attraction occurs in solution between the cationic CTAB and anionic YZr acetatoglycolate. Upon later addition of La/Sr/Mn salts to the alkaline mixture, charged hydroxo species are formed and experience an electrostatic attraction toward the YZr acetatoglycolate/CTAB interface.[33] Eventual precipitation is slowly reached resulting in a material

(31) Tian, Z. R.; Tong, W.; Wang, J. Y.; Duan, N. G.; Krishnam, V. V.; Suib, S. L. *Science* **1997**, *276*, 926.

(32) (a) Luo, J.; Huang, A.; Park, S. H.; Suib, S. L.; O'Young, C. L. *Chem. Mater.* **1998**, *10*, 1561. (b) Luo, J.; Zhang, Q.; Suib, S. L. *Inorg. Chem.* **2000**, *39*, 741.

Table 2. Average Particle Sizes of YSZ and $La_{1-x}Sr_xMnO_3$ Phases

nc-LSMYSZ				*meso*-YSZ	
$(Y,Zr)O_2$, f c c		$La_{1-x}Sr_xMnO_3$, R $\bar{3}$ C		$(Y,Zr)O_2$, f c c	
hkl	size (nm)	hkl	size (nm)	hkl	size (nm)
1 1 1	89 (1)	0 1 2	108 (4)	1 1 1	337 (6)
2 0 0	109 (4)	1 1 0	71 (2)	2 0 0	215 (5)
2 2 0	78 (1)	0 1 4	84 (2)	2 2 0	664 (8)
3 1 1	72 (1)	1 1 3	92 (19)	3 1 1	427 (2)
2 2 2	60 (3)	0 2 2	92 (3)	2 2 2	418 (2)
4 0 0	69 (4)	0 0 6	56 (4)	4 0 0	491 (2)
		0 2 4	79 (1)		
		1 2 2	51 (6)		
		1 1 6	55 (8)		
		3 0 0	44 (1)		
		0 1 8	66 (4)		
		2 2 0	52 (2)		
		0 2 8	49 (2)		

that can best be described as an organic/inorganic composite mesostructure containing a cationic surfactant template and pore walls formed from partially hydrolyzed YZr acetatoglycolate. Nanoscale La/Sr/Mn hydroxides and oxo-hydroxides are believed located near or at the YZr pore walls and the surfactant headgroup region. We believe the addition of CTAB leads to an organization of the charged precursors in such a way that a phase separation at the nanoscale must exist between the YZr acetatoglycolate and the La/Sr/Mn species. Evidence for this is observed from "control experiment B" where the surfactant is excluded from the reaction mixture resulting, upon calcination to 800 °C − 1100 °C, in the formation of large amounts of unwanted products such as La_2O_3 (JCPDS card 22-0369), $La(OH)_3$ (JCPDS card 6-0585), and other complex oxides, possibly La/Mn pyrochlores, along with the desired phases of cubic YSZ and LSM perovskite. The nanoscale phase separation created by CTAB in solution allows for the YZr acetatoglycolate and La/Sr/Mn hydroxides to remain concentrated in different regions of the as-synthesized product so that each phase can later separately crystallize as cubic YSZ at 450 °C and LSM perovskite above 800 °C as presented in Scheme 2.

Figure 7 shows SEM micrographs of a nc-LSMYSZ sample supported on the dense YSZ substrate after analysis by impedance spectroscopy. The thickness of the electrode layer is about 40 μm as seen in cross-section of the electrode in the micrograph at the top left. Figure 8 compares typical complex impedance spectra recorded at 800 °C for three different nc-LSMYSZ samples and a 50:50 LSM/YSZ physical mixture by weight (denoted cLSMYSZ). Each of the three nc-LSMYSZ

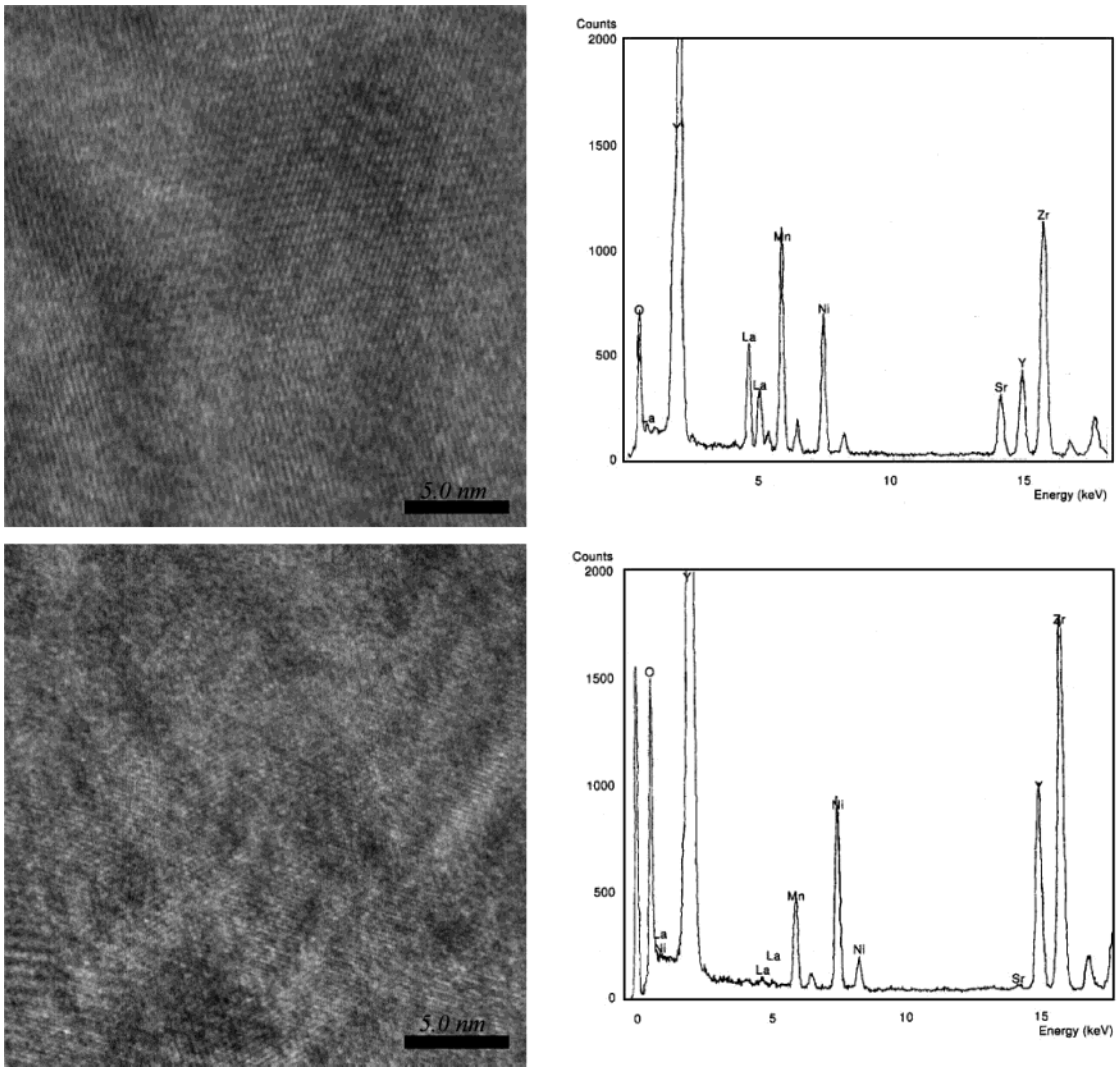

Figure 5. HR−FE-STEM micrographs and corresponding EDX spot analysis spectra of sample regions denoted as "phase P" (top) and "phase YSZ" (bottom). The peak for Ni is due to the TEM grid.

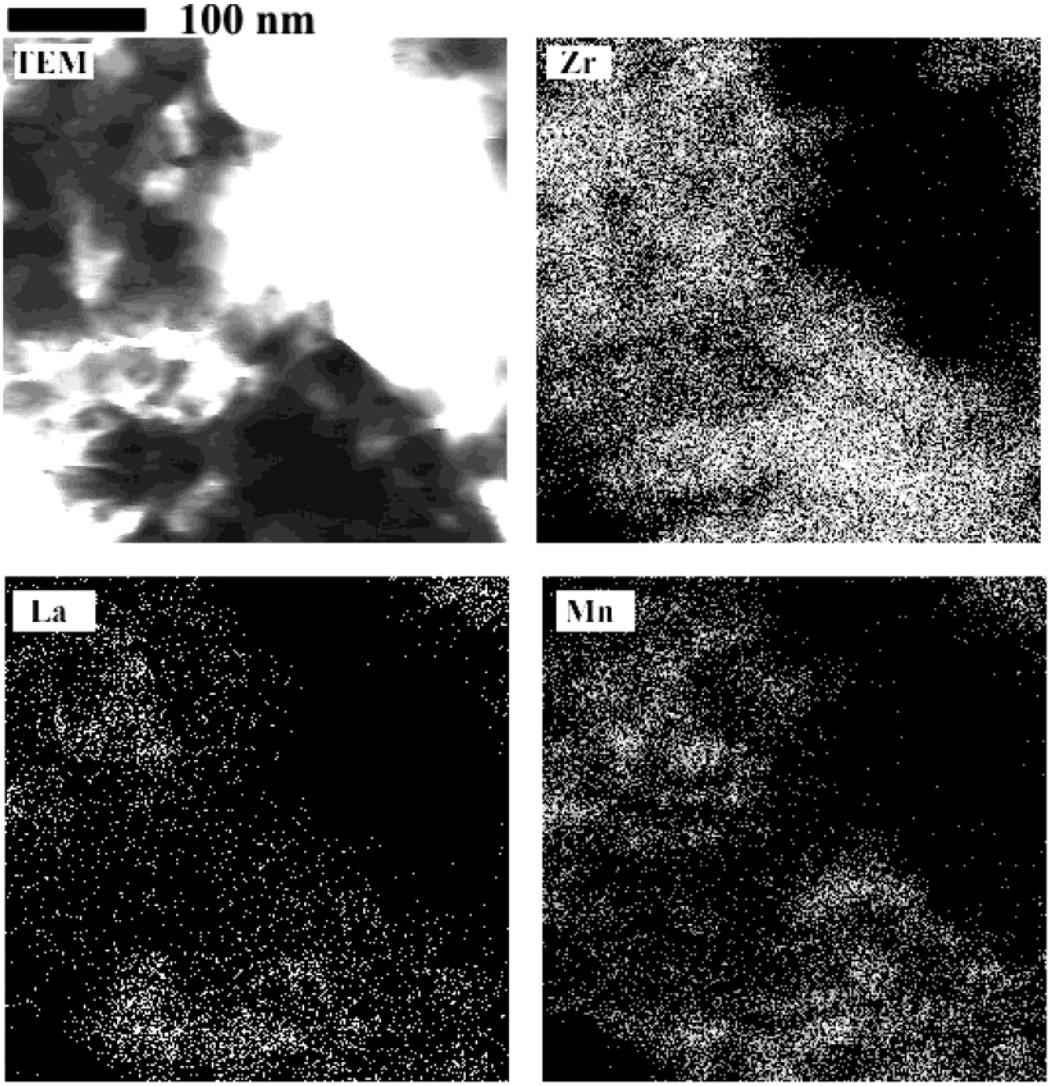

Figure 6. TEM micrograph and corresponding EDX maps (Zr Kα, La Lα, and Mn Kα) of a nc-LSMYSZ thin section.

Scheme 2. Structural Evolution of *meso*-LSM-YSZ to nc-LSMYSZ upon Sintering[a]

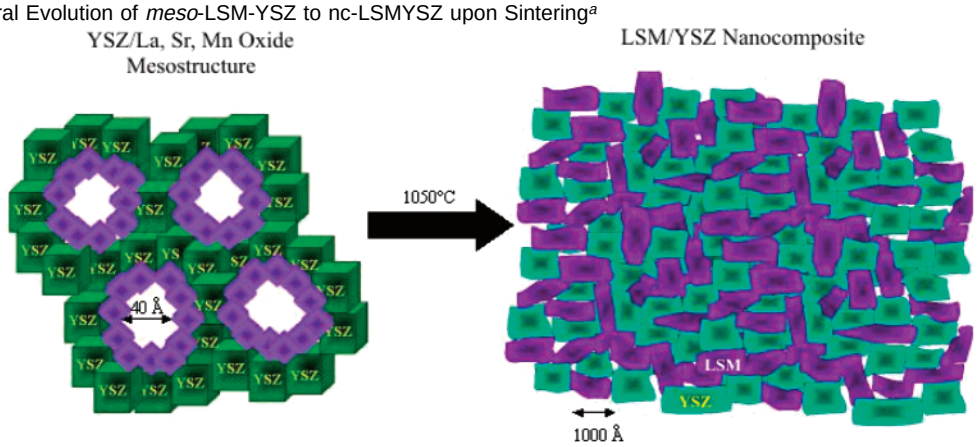

[a] The purple species in the mesostructure represent poorly crystalline La, Sr, and Mn oxides.

spectra appear to be composed of two visually separable arcs, whereas the spectra of the LSM/YSZ physical mixture appears asymmetric and may be composed of two arcs which overlap. The high frequency arc is often interpreted in the literature to oxygen transfer within YSZ as it does not vary with oxygen partial pressure and has an activation energy similar to YSZ (about 1 eV). The low frequency arc is usually attributed to the electrochemical reduction of oxygen because it is reported to be dependent on oxygen partial pressure. This process is most often reported as having an activation energy of 1.8 to 1.9 eV, however, Steele reports that it should be closer to 1.4 eV.[4c,34] These two processes make up the total polarization resistance

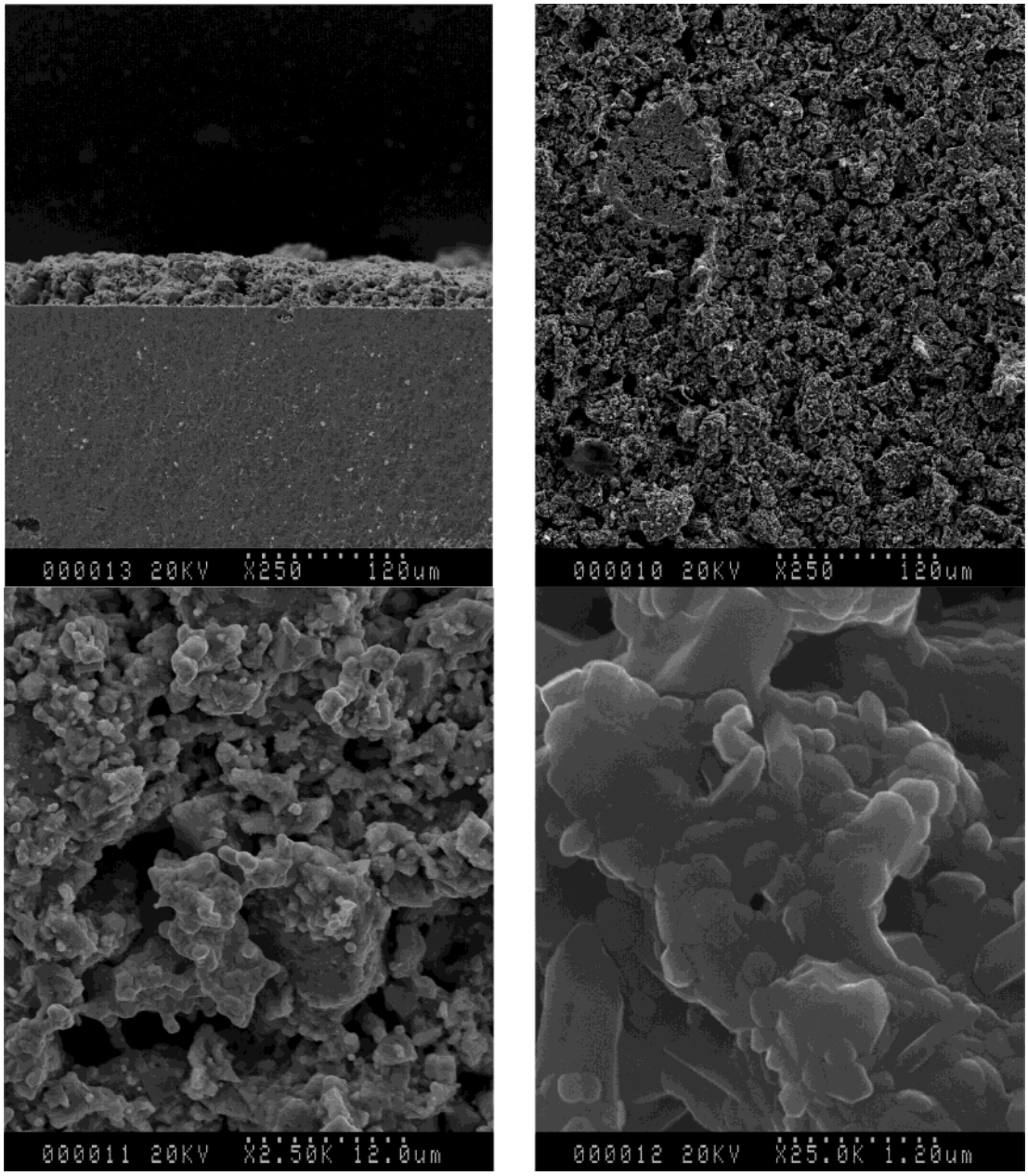

Figure 7. SEM micrographs after analysis by impedance spectroscopy for the nc-LSMYSZ sample "3LSMYSZ" supported on a dense YSZ substrate. The top, left image represents a cross-section of the sample, whereas the other images are top views at different magnifications.

(R_p) of the sample, and this was determined from the difference between the high frequency and low-frequency intercepts of the best fitting arcs. Arrhenius plots for R_p are shown in Figure 9 for two nc-LSMYSZ samples and the LSM/YSZ physical mixture. The apparent activation energies (E_a) for both nc-LSMYSZ samples correlate closely, resulting in an E_a of 1.45 and 1.42 eV, respectively. These are slightly lower than that of the LSM/YSZ physical mixture, which has an E_a of 1.53 eV.

Table 3 summarizes our findings for four representative nc-LSMYSZ samples and the 50:50 LSM/YSZ physical mixture sample. The resistance determined from the high-frequency intercept is referred to as the series resistance (R_s) and can be ascribed to the sum of lead wire resistances, bulk resistance of the electrolyte, and the quality of physical contact between the fired sample and electrolyte. A careful analysis by PXRD, XRF, magnetic susceptibility of each sample helps to rationalize our findings. First, sample 1LSMYSZ contains the most significant amount of impurity phases, which is reflected in higher values observed for R_s and R_p as well as E_a. It is evident from this relatively high resistivity and activation energy that the impurity phases disrupt both the electronic and ionic pathways within the electrode. Sample 18LSMYSZ contains much less of the LSM perovskite phase than the other samples, hence this is also reflected in terms of its higher resistances and activation energy, as a continuous network of LSM is not likely to be achieved at this low loading. Samples 64LSMYSZ and 3LSMYSZ compared best to the LSM/YSZ physical mixture sample and even gave a lower activation energy, however, there appears to be a

(33) (a) Chanaud, P.; Julbe, A.; Vaija, P.; Persin, M.; Cot, L. *J. Mater. Sci.* **1994**, *29*, 4244. (b) Dibtseva, N. M.; Kienskaya, K. I.; Nazarov, V. V. *Colloid J.* **2001**, *63*, 150. (c) Felmy, A. R.; Dixon, D. A.; Rustad, J. R.; Mason, M. J.; Onishi, L. M. *J. Chem. Thermodyn.* **1998**, *30*, 1103.
(34) Steele, B. C. H. *Solid State Ionics* **1996**, *86*−*88*, 1223.

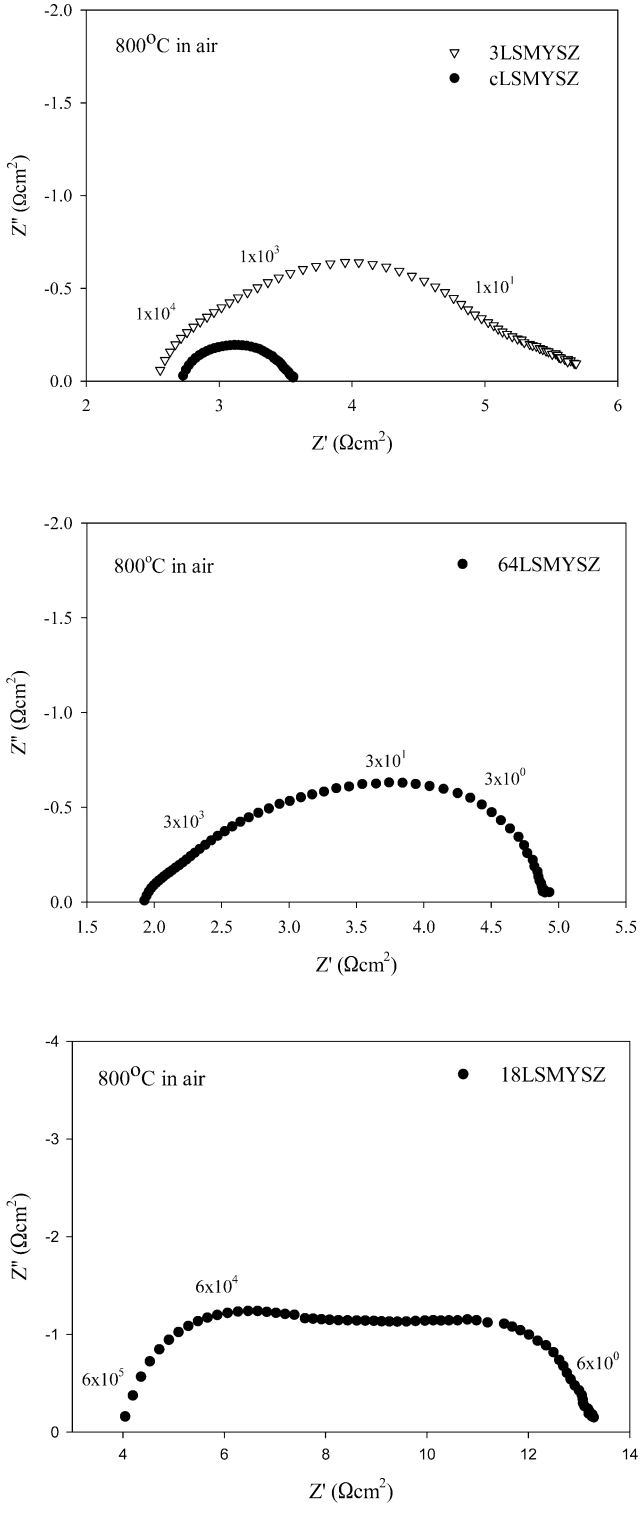

Figure 8. Complex impedance plots for three different nc-LSMYSZ samples and a 50:50 LSM/YSZ physical mixture sample (top plot), denoted cLSMYSZ.

discrepancy between their performances as an electrode and the relative amount of perovskite phase present in the material. Upon analyzing each material by XRF, sample 64LSMYSZ had a La/Sr/Mn stoichiometry close to the desired 0.7:0.3:1 ratio while sample 3LSMYSZ was quite deficient in strontium. This would lower the relative percentage of Mn^{4+} sites in the perovskite, leading to semiconducting behavior and lower activity as an air electrode. A comparison of sample 64LSMYSZ with the

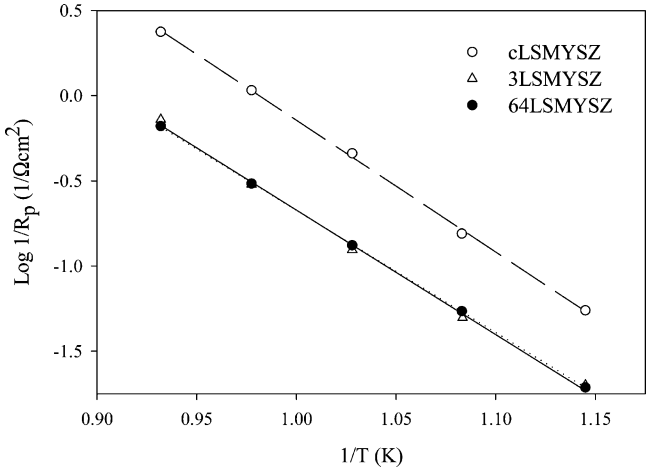

Figure 9. Arrhenius plots comparing nc-LSMYSZ samples (3LSMYSZ and 64LSMYSZ) to a composite made from mechanically mixing commercially bought LSM and YSZ powder (denoted cLSMYSZ).

Table 3. Findings for Four Representative nc-LSMYSZ Samples and the 50:50 LSM/YSZ Physical Mixture Sample

sample	relative wt % *P* phase	series resistance, R_s (Ωcm²)	polarization resistance, R_p (Ωcm²)	activation energy, E_a (eV)
CLSMYSZ	50	2.71	0.42	1.53
1LSMYSZ	44	10.18	16.05	1.67
3LSMYSZ	56	2.53	1.38	1.45
18LSMYSZ	14	3.93	4.70	1.63
64LSMYSZ	35	1.92	1.51	1.42

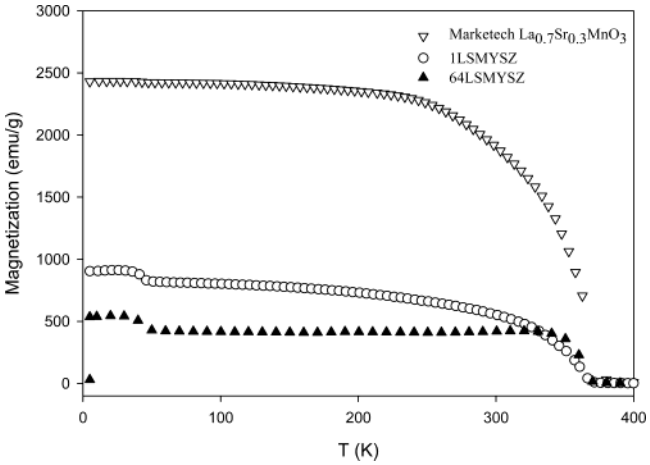

Figure 10. Magnetization as a function of temperature plots comparing the commercially obtained LSM powder and two nc-LSMYSZ composite samples.

physical mixture sample, cLSMYSZ, shows that the physical mixture material has a slightly lower R_p, however this material contains a higher LSM content by approximately 15 wt %. These results indicate promise in the compositional tunablity of nc-LSMYSZ materials in terms of relative loading of LSM, stoichiometry of LSM, and elimination of undesirable impurity phases, which bodes well for improved performance electrodes.

A magnetic susceptibility comparison of these samples is presented in the form of magnetization versus temperature plots shown in Figure 10. The composite samples 1LSMYSZ and 64LSMYSZ each exhibit a ferromagnetic transition temperature, T_c, close to that for the commercially purchased $La_{0.7}Sr_{0.3}MnO_3$ powder (99.9%, 1−10 μm particle size, Marketech International,

Inc.) of around 360 K. A comparison of the saturation magnetization values for each sample shows that they are quite similar to one another if one takes into account the total weight percent loading of the LSM perovskite phase in each sample, 100% for the commercial sample, 44% for 1LSMYSZ, and 35% for 64LSMYSZ, respectively. Interestingly, the sample 3LSMYSZ (not shown in Figure) exhibits a much lower T_c of 210 K, which is indicative for lower Mn^{4+} content.[10] These results give conclusive evidence for the assumed stoichiometry as determined from XRF analysis and our space group determination of the LSM phase in our nc-LSMYSZ materials. XRF analysis is a bulk elemental analysis technique, thus it is difficult on the basis of XRF alone to assume the stoichiometry of the LSM perovskite phases.

In an attempt to investigate the electrochemical stability of nc-LSMYSZ electrodes under cell operating conditions, we examined a cell composed of nc-LSMYSZ/YSZ/Pt under a cathodic polarization of −0.3V versus a Pt reference electrode (see the Experimental Section "g" for details). The nc-LSMYSZ sample chosen to be investigated as the working electrode was "64LSMYSZ", which we deemed to have the optimal LSM stoichiometry, low impurity content, and the lowest activation energy of all the samples investigated above. The top of Figure 11 portrays the cell current density over a period of about 40 h. An increase in current density was observed over the first 20 h up to almost 1 A·cm^2, following which the cell operation was interrupted in order to perform various I−V tests and upon resumption of cathodic polarization at −0.3V, a drop in current density was observed mainly due to electrochemical prehistory effects.[35] Finally, the cell reached a steady current density at 0.65 A·cm^2 until the end of the test, which is close to the initial current density of 0.67 A·cm^2. Impedance spectra were measured at both −0.3V and OCV during regular intervals during the 40 h cathodic polarization test. The bottom of Figure 11 illustrates the change in impedance spectra taken at OCV over operation time, and a summary of the series and polarization resistances along with the cell current density are reported in Table 4. The resistance values here are lower than that reported from studies using the symmetrical cell design reported in Table 3 mainly due to the use of a reference electrode and shorter lead wires.

The initial R_p values compares well to values achieved by Bagger of 70 mΩ cm^2 to 120 mΩ cm^2 at 850 °C for functionally graded LSM/YSZ composite cathodes.[3] Both R_s and R_p are observed to increase over operation time as evident from the shift of complex impedance semicircles to higher values. Two possible sources for the small increase in overall cell resistance may originate from a sintering of the LSM/YSZ composite or the formation of reaction products at the LSM/YSZ interfaces within the 3-D network of the composite or at the cathode/electrolyte interface. The sintering of the composite cathode during operation may decrease the TPB length due to a densification of the electrode causing a concomitant decrease its electrochemical activity. This process may or may not pose a problem depending on if the system reaches thermodynamic equilibrium without a significant increase in cell resistance. On the other hand, the formation of reaction products at the LSM/YSZ interface is most serious as this can interrupt electron and ion transport within the composite cathode and ion transport between the cathode and electrolyte. This issue will be further examined in the discussion below. A third and equally probable explanation for the observed increase in cell resistance can be related to the gold ink used to make contact to the working electrode. A study by Guillodo et al. of metal ink-based current collectors for SOFC cermet anodes found that much diffusion of gold particles had occurred at elevated temperatures resulting in a doubling of the polarization resistance over a period of 24 h.[36] Future studies making use of a cell designed for electrical contact to the working electrode with only the pressure contact of platinum mesh may prove useful in eliminating this deleterious effect.

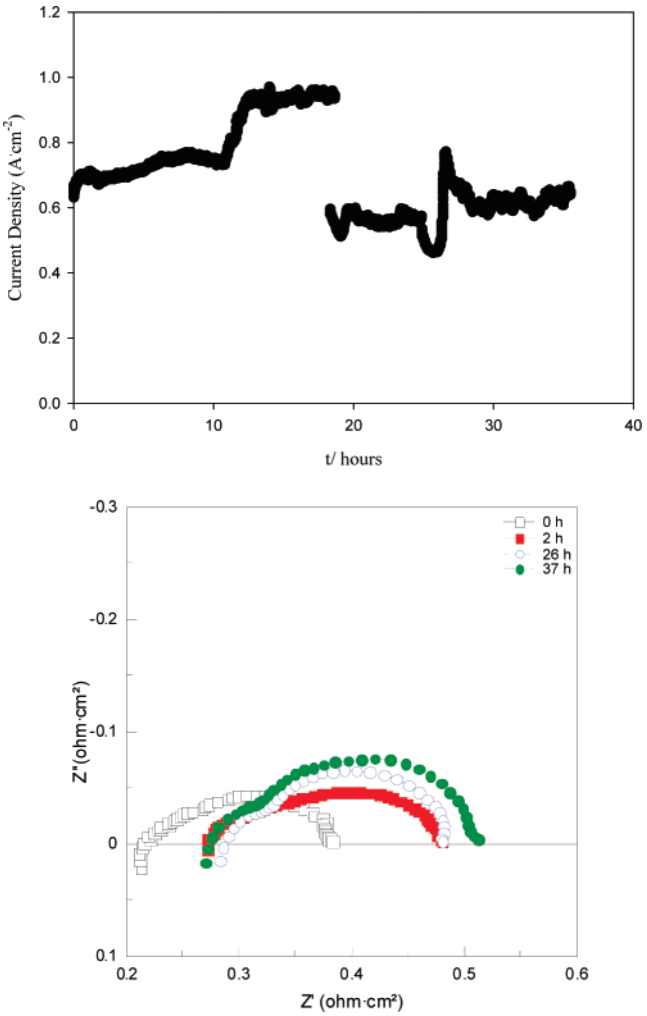

Figure 11. Top- Current density test of "64LSMYSZ"/YSZ/Pt under a constant applied voltage (E = −0.3V) at 800 °C. Bottom- Complex impedance plots taken at OCV during time intervals of the current density test.

Table 4. Series and Polarization Resistances along with the Cell Current Density

	OCV		−0.3V		
time (h)	R_s (Ωcm^2)	R_p (Ωcm^2)	R_s (Ωcm^2)	R_p (Ωcm^2)	current density (A·cm^2)
0	0.22	0.17	0.26	0.14	0.67
38	0.27	0.24	0.33	0.35	0.65

(35) Juhl, M.; Mogensen, M.; Jacobsen, T.; Zachau-Christiansen, B.; Thorup, N.; Skou, E. *Proc. 4th Int. Symp. SOFC*, Yokohama, Japan, **1995**, 554.

(36) Guillodo, M.; Vernoux, P.; Fouletier, J. *Solid State Ionics* **2000**, *127*, 99.

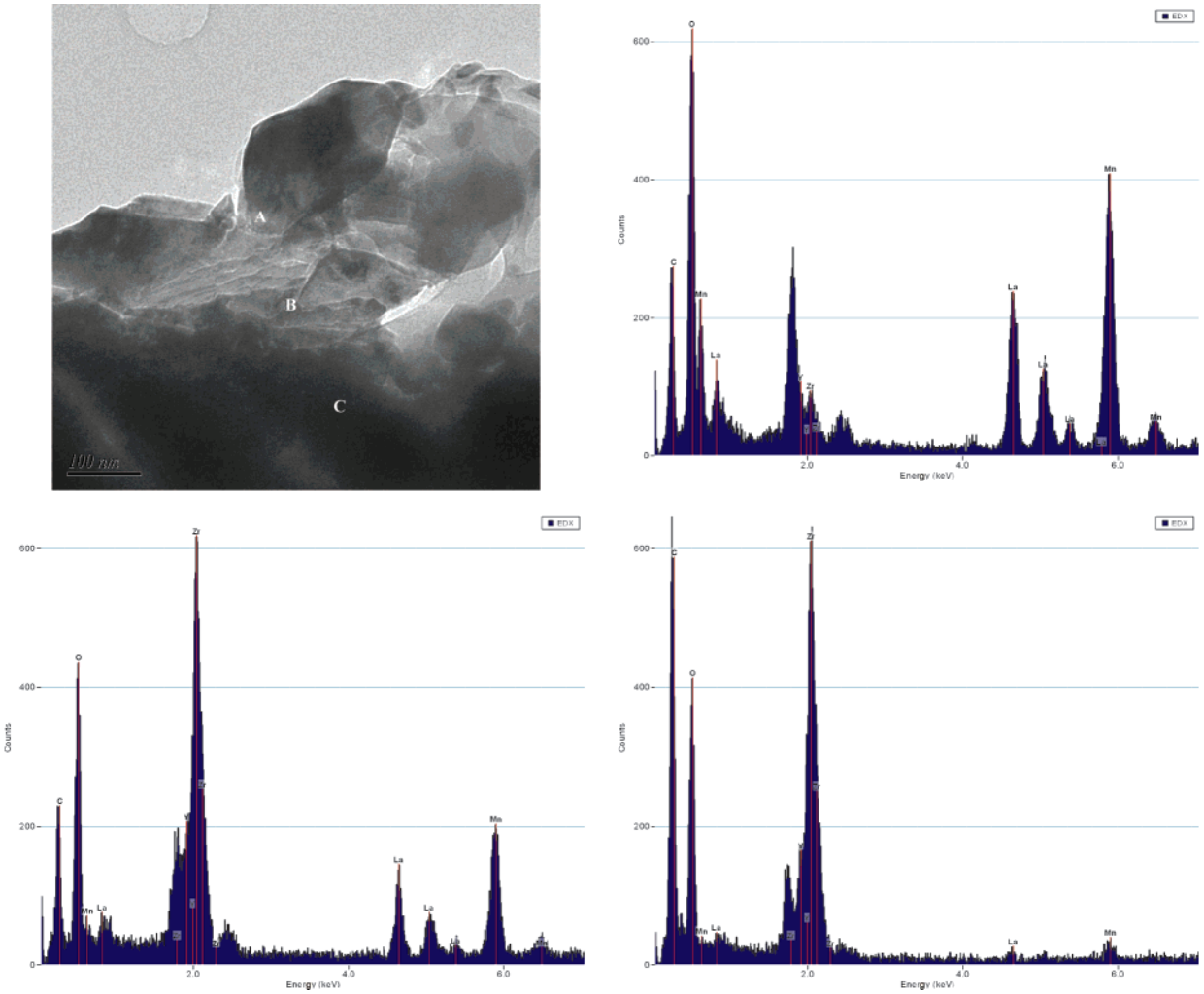

Figure 12. TEM micrograph for a thin section of the cathode/electrolyte interface and EDX spot analyses corresponding to the spots labeled as "A", "B", and "C" in the micrograph.

To probe the solid state diffusion of Mn or La into the YSZ electrolyte and the possible formation of the unwanted, highly resistive phases of $La_2Zr_2O_7$ and $SrZrO_3$, we have investigated the cathode/electrolyte interface by TEM imaging and EDX spot analysis, as shown in Figure 12. The analysis of the cathode/electrolyte interface by TEM was quite a challenging task, as in order to procure electron transparent thin sections of the cathode/electrolyte interfacial region, much of the cathode and electrolyte away from the interface must first be mechanically removed by microtome. Several thin sections of approximately 60 nm thickness were investigated by EDX spot analysis (electron beam probe size of approximately of 20 nm) showing an excellent transition across the interface, where the representative spots are labeled in the TEM micrograph as "A", "B", and "C". Spot "A" represents the composite cathode near the interface and shows a high relative percentage of Mn and La compared to Zr. The relative amount of La to Mn is close to the 0.7:1.0 ratio supported by XRF, PXRD, and magnetic susceptibility. As we approach closer to the interface by approximately 100 nm (spot "B"), the relative amount of La and Mn decreases, but remains in the same 0.7 to 1.0 ratio, with a dramatic increase in the relative percentage of Zr. At spot "C", roughly 100 nm from spot "B", very low levels of Mn and even lower levels of La are observed in comparison to Zr. This may be indicative of low level of interfacial diffusion of Mn, and to a lesser extent La, at the 100 nm length scale forming a solid solution with YSZ. None of the regions analyzed show a 1:1 ratio of La to Zr and, thereby, do not support the presence of $La_2Zr_2O_7$. Additionally, upon analyzing the composite cathode/electrolyte interface by PXRD after the 40 h current density test, we did not observe any growth in the already present minor impurity phases discussed in Figure 4, nor did we observe the formation of any new phases.

The interfacial diffusion of Mn, La, and Sr has been widely studied by many researchers, however, most studies were done at the micron length scale using SEM/EDX.[37] The few studies where TEM/EDX was used, the sample consisted of either mixed powders of LSM and YSZ that have been pressed and sintered into pellets[4g] or samples where the LSM cathode layer has been etched away from its dense YSZ substrate by the use of a strong mineral acid.[38] In both types of analyses, the overwhelming message from these reports is that an A-site deficient LSM cathode, and even excess Mn in the form of its pure oxide, as well as using low sintering temperatures ($\leq$1100 °C) can inhibit the formation of $La_2Zr_2O_7$ and $SrZrO_3$ to a great

(37) See for example: Kleveland, K.; Einarsrud, M.-A.; Schmidt, S.; Faaland, S.; Wiik, K.; Grande, T. *J. Am. Ceram. Soc.* **1999**, *82*, 729.
(38) Mitterdorfer, A.; Gauckler, L. J. *Solid State Ionics* **1998**, *111*, 185.

extent. As our nc-LSMYSZ materials appear to have an excess of Mn, (not altogether surprising because the initial molar ratio of starting reagents was 1 Mn: 0.34−0.42 La:0.24−0.30 Sr) either in the form of a solid solution with YSZ or as the phase Mn_2O_3, this may bode well for the long term stability of our materials. However, long-term electrochemical studies (>400 h) are required in order to fully investigate the stability of our materials.

Conclusion

LSM/YSZ nanocomposites, nc-LSMYSZ, have been prepared from the intentional structural collapse of a mesoporous product formed from the surfactant-based co-assembly of yttrium−zirconium acetatoglycolate and inorganic salts of La^{3+}, Sr^{2+}, and Mn^{2+}. Careful control of the stoichiometry of the LSM reagents in the aqueous synthesis determines the phase purity of the LSM perovskite and doping level of strontium. These materials consist of interpenetrating networks of rhombohedral LSM and cubic YSZ phases, which have an average crystallite size of less than 100 nm. Analysis by impedance spectroscopy demonstrates the importance of eliminating the lanthanum oxide-based impurity phases, while optimizing both the strontium content and total percent loading of LSM. Representative nc-LSMYSZ samples exhibit lower activation energy than the composite cathode prepared from commercially available powders and a low polarization resistance at 800 °C. Further optimization may lead to enhanced performance SOFC composite cathodes, which may lower the working temperature.

Note Added after ASAP: In the version published on the Web 4/3/2003, the units for R_s and R_p in the column heading of Table 4 were incorrect. The final Web version published 4/3/2003 and the print version are correct.

JA027881P